Available online at www.sciencedirect.com

SciVerse ScienceDirect

Ceramics International 39 (2013) 6237–6249

CERAMICS INTERNATIONAL

www.elsevier.com/locate/ceramint

Cutting characteristics of dental glass ceramics during *in vitro* dental abrasive adjusting using a high-speed electric handpiece

Xiao-Fei Song[a,*], Ling Yin[b], Jian-Hui Peng[a], Bin Lin[a]

[a]*Key Laboratory of Advanced Ceramics and Machining Technology of Ministry of Education, School of Mechanical Engineering, Tianjin University, Tianjin 300072, China*

[b]*School of Engineering and Physical Sciences, James Cook University, Townsville, Queensland 4811, Australia*

Received 8 November 2012; received in revised form 11 January 2013; accepted 12 January 2013
Available online 23 January 2013

Abstract

Machinability is an important characteristic of dental ceramics for restorative dentistry because machining is not only commonly employed in dental CAD/CAM systems but also essential in dental adjustments for occlusal fitting and restorative quality. This paper reports on an *in vitro* study on machinability of dental ceramics by quantifying cutting characteristics of feldspar and leucite glass ceramics in simulated dental adjusting using a high-speed electric handpiece and diamond burs. Cutting forces, force ratio, energy, surface integrity and bur topography were evaluated as functions of clinically relevant cutting conditions. The results indicate that tangential and normal forces and specific cutting energy for both materials exhibited significant dependences ($p < 0.01$) on both the bur depth of cut and the bur feed rate. Surface roughness showed a weak influence by the choice of the material ($0.05 > p > 0.01$) but no correlations with the cutting conditions applied ($p > 0.05$). At the slower feed rates or smaller depths of cut the cutting behaviors for the two materials were very similar in terms of cutting forces and specific cutting energy. At the deeper depths of cut or faster feed rates, normal forces for leucite glass ceramic were significantly higher than those for feldspar glass ceramic ($p < 0.01$). However, leucite glass ceramic produced better cutting surfaces with less fracture areas compared with feldspar ceramic due to its lower index of brittleness and higher force threshold for brittle–ductile transition. This research provides a methodological qualification in evaluating cutting characteristics of dental ceramics and quality control in clinical dentistry.

Keywords: Dental glass ceramics; Electric handpiece; Cutting forces; Machinability; Surface integrity

1. Introduction

Glass ceramics have been increasingly used in restorative dentistry because of their biocompatibility and esthetic attraction [1,2]. They are clinically used as veneers, crowns, bridges and fixed partial dentures depending on functional and esthetic demands [3]. These dental ceramics include feldspar, leucite, lithium disilicate, mica, alumina, and fluorapatite glass ceramics [4,5]. Due to different reinforced crystals in glass matrixes, dental glass ceramics have very different mechanical properties and behaviors [6]. Among these materials, feldspar and leucite glass ceramics most widely serve as veneers, inlays, onlays, three quarter crowns and possibly bicuspid crowns due to their approximation to the appearances of human enamels [7]. Recent studies have shown that restorative ceramics had failure rates of less than 5% at 5 years resulting from loss of retention or fracture [8]. Feldspar glass ceramic veneers revealed long survival rates of 93% at 10 years [9] and 94.4% at 12 years [10]. Veneers made of leucite glass ceramic had a success rate of 98.8% after 6 years [11]. Despite improved longevities, strength limitation of glass ceramics is still a distinct obstacle to expand clinical applications because of their inherent brittleness and poor machinability [12].

Machinability is a very important characteristic of dental materials, especially for brittle glass ceramics [13]. This is because abrasive cutting operations are commonly involved during machining of all-ceramic framework and adjusting of ceramic prostheses by dentists and technicians

*Corresponding author. Tel.: +86 22 8740 1639; fax: +86 22 2740 4915.
E-mail address: xiaofeisong@tju.edu.cn (X.-F. Song).

0272-8842/$ - see front matter © 2012 Elsevier Ltd and Techna Group S.r.l. All rights reserved.
http://dx.doi.org/10.1016/j.ceramint.2013.01.045

[13,14]. Poor machinability of a material not only affects the quality of prostheses but also results in low economic efficiency [13]. Bulk glass ceramics are generally machined using dental CAD/CAM systems to form basic shapes of prostheses [15]. Then occlusal interfaces or areas must be adjusted intraorally or extraorally for occlusal fits using clinical dental handpieces with abrasive burs [15–17]. Both the CAD/CAM processing and adjusting using abrasive burs involve surface machining and material removal, inevitably inducing surface and subsurface damage in ceramic restorations [15–17]. Studies have shown that the machining-induced damage in brittle ceramics has been the primary cause of failure in ceramic restorations [15,18,19]. Therefore, the fundamental understanding of the ceramic cutting characteristics in dental abrasive adjusting is highly required for improved machinability and good prosthetic quality in restorative dentistry.

In dental adjusting with abrasive burs, air turbine high-speed handpieces have been used in dental cutting for more than 40 years [16]. They are the most popular type of clinical handpieces owing to their ability to cut tooth structure rapidly, good ergonomic weights and sizes, low risk of pulpal damage and ease of repair [20–22]. However, loud noises, vibrations, and poor concentricity have been disadvantages in applying air turbine high-speed handpieces [23]. More recently, electric motor high-speed handpieces were invented to overcome disadvantages of air turbine high-speed handpieces. These new type handpieces can be operated at constant rotating speeds and high torques with very little stalling [20,24]. They induce much less noises and vibrations [20,24]. Studies also show that cutting efficiencies of enamel for cavity preparation using electric handpieces were higher than those using air-turbine handpieces [25], especially when applying carbide burs [26]. However, there is little research on quantitative cutting characteristics of dental ceramics using high-speed electric handpieces. These missing characteristics are, in fact, essential to materials selection, processing and restorative success in dental practice.

The aim of this paper was to investigate machinability of two popular dental ceramics, feldspar and leucite glass ceramics, by conducting *in vitro* cutting in simulated dental adjusting using a high-speed electric handpiece and coarse diamond burs. Normal and tangential cutting forces, force ratio, specific cutting energy, surface roughness and surface morphology were quantitatively characterized as functions of relevant clinically dental cutting operational variables. Surface fracture and generation mechanisms were also discussed with respect to index of brittleness, force thresholds for brittle–ductile transition and chip geometry.

2. Materials and methods

2.1. Sample preparation

Two popular machinable feldspar and leucite glass ceramics in restorative dentistry were subject to this investigation. The

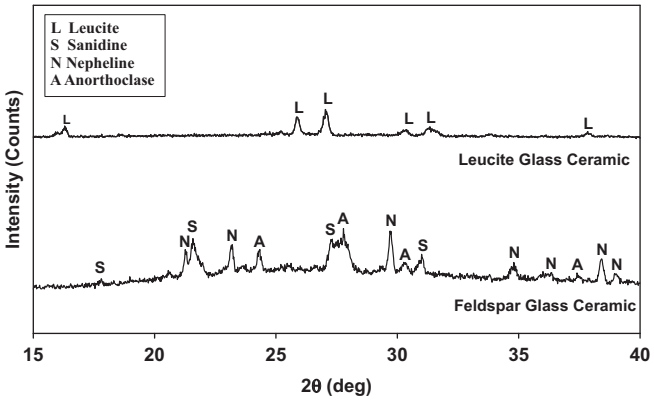

Fig. 1. X-ray diffraction patterns of the feldspar and leucite glass ceramics.

X-ray diffraction patterns of these two materials are shown in Fig. 1. The feldspar glass ceramic (Vita Mark II, Vita Zahnfabric, Germany) was composed of glass matrix and irregular feldspar crystals of sanidine, nepheline and anothoclase (Fig. 1) with sizes of 1–7 μm [27,28]. Reported mechanical properties of the material are: Vickers hardness $H=6.2$ GPa, Young's modulus $E=68$ GPa, fracture toughness $K_{IC}=0.9$ MPa $m^{1/2}$, and flexural strength $\sigma=100$ MPa [29]. The leucite glass ceramic (IPS ProCAD, Ivoclar vivadent, Liechtenstein) contained glass matrix and leucite crystals (Fig. 1) with sizes of approximately 5–10 μm [30]. Reported mechanical properties of the material include Vickers hardness $H=5.6$ GPa, Young's modulus $E=70$ GPa, fracture toughness $K_{IC}=1.3$ MPa $m^{1/2}$, and flexural strength $\sigma=127$ MPa [31]. Specimens were all ground and polished with dimensions of 15 mm × 12 mm × 5 mm. Each surface of 12 mm × 5 mm was attached with a metal stick for fixing the specimen in cutting process.

2.2. In vitro dental cutting procedure

A two-dimensional computer-assisted cutting apparatus described previously [32] was modified for the current dental cutting testing. The new overall experimental setup is shown in Fig. 2(a). It consisted of a dental electric motor (NL400, NSK, Japan), an electric handpiece (Ti95L, NSK, Japan), a three-dimensional, piezoelectric force dynamometer (9257 A, Kistler, Switzerland), a charge amplifier (5070 A, Kistler, Switzerland), and a high-speed data acquisition system (DynoWare, Kistler, Switzerland). Burs (211, ISO 110524014, Shofu, Japan) applied in cutting were cylindrical, coarse diamond with a 106–125 μm grit size, a 1.4 mm diameter (d_s) and a 7-mm cutting length (l). The electric handpiece was driven at a 0.35 MPa air pressure and the water coolant was supplied to the cutting area at a 30 ml/min flow rate. The 7-mm diamond portion of the bur was used to cut the specimen surface of 12 mm × 5 mm at the bur rotational speed of 200 krpm, depths of cut of 10–60 μm and feed rates of 15–75 mm/min. A detailed illustration of dental bur-specimen movement is shown in Fig. 2(b).

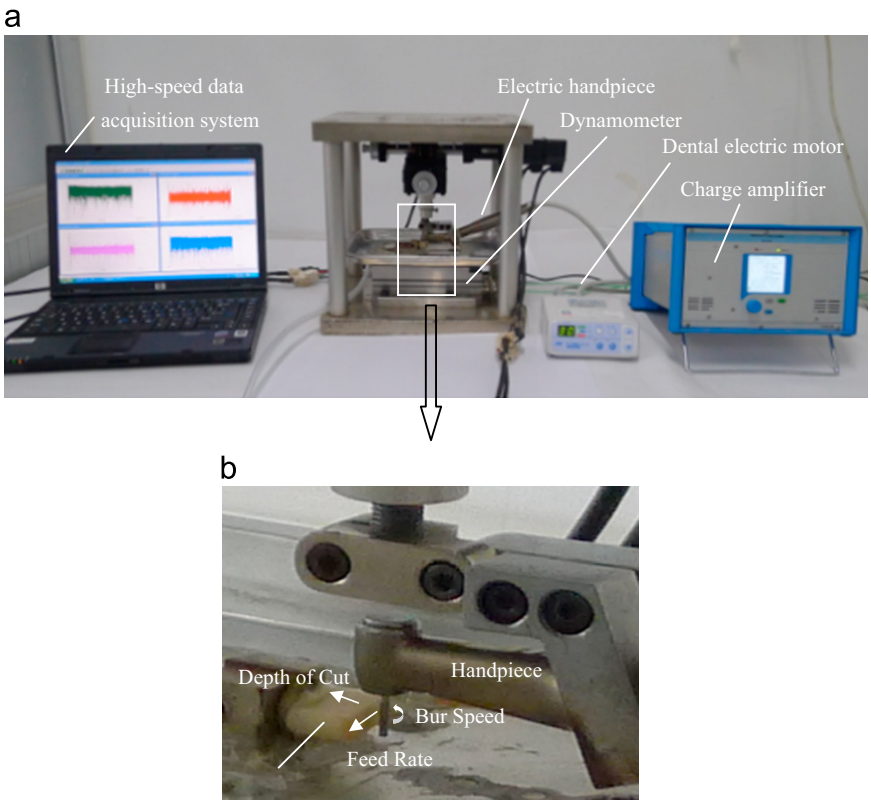

Fig. 2. (a) Overall experimental setup for *in vitro* dental cutting and (b) detailed illustration of dental handpiece/bur-specimen movement.

2.3. Characterization of cutting process

Three cutting passes were operated to insure the steady state prior to the force measurement. Details of these measurements were described previously [32]. Briefly, both tangential and normal dynamic forces were measured using the dynamometer. The specific cutting energy u was determined as [33]

$$u = F_t v_s / a v_w b \quad (1)$$

where F_t is the tangential cutting force, v_s is the cutting speed, a is the depth of cut, v_w is the feed rate, and b is the thickness of the specimen. Under each cutting condition, three measurements were conducted for mean values and their standard deviations of cutting forces, force ratio and specific cutting energy.

Both arithmetic mean surface roughness R_a and maximum roughness R_{max} were measured with a stylus profilometer (Taylor Hobson, UK). Measurement was performed perpendicular to the cutting direction at 0.25 mm cut-off length and 1.25 mm traverse length. Selected machined ceramic surfaces and new and used diamond burs were sputtered with gold and observed using a scanning electron microscope (Nanosem 430, FEI, USA). A two-way analysis of variance (ANOVA) F-test at a 5% significant level was applied to evaluate the effects of materials and operational parameters on cutting characteristics.

3. Results

3.1. Cutting forces and force ratio

Tangential cutting forces versus depth of cut for feldspar and leucite ceramics at the feed rates of 15 mm/min and 75 mm/min are shown in Fig. 3(a). The results reveal that tangential forces increased with the depth of cut for both feldspar and leucite ceramics at all the feed rates ($p < 0.01$). The force values in the range of 0.34–1.07 N obtained at the higher feed rate of 75 mm/min were larger than the values 0.30–0.75 N at the lower feed rate of 15 mm/min. Fig. 3(b) shows tangential forces versus feed rate for the two materials at the depths of cut 10 μm and 60 μm. It demonstrates that tangential forces for the two materials increased with the feed rate and the force values are significantly higher at the larger depth of cut ($p < 0.01$). For instance, at the 10-μm depth of cut, the forces were about 0.3 N and at the 60-μm depth of cut, the forces increased to approximately 0.8–1.1 N, 3 or 4 times higher. In comparison between the two materials, the forces for leucite ceramic were slightly higher than those for feldspar ceramic.

Normal forces versus depth of cut for feldspar and leucite ceramics at the feed rates of 15 mm/min and 75 mm/min are plotted in Fig. 4(a). It shows that normal forces for the two materials increased with the depth of cut and the increase rates were higher at the higher feed rates ($p < 0.01$). It also shows that the forces for leucite ceramic

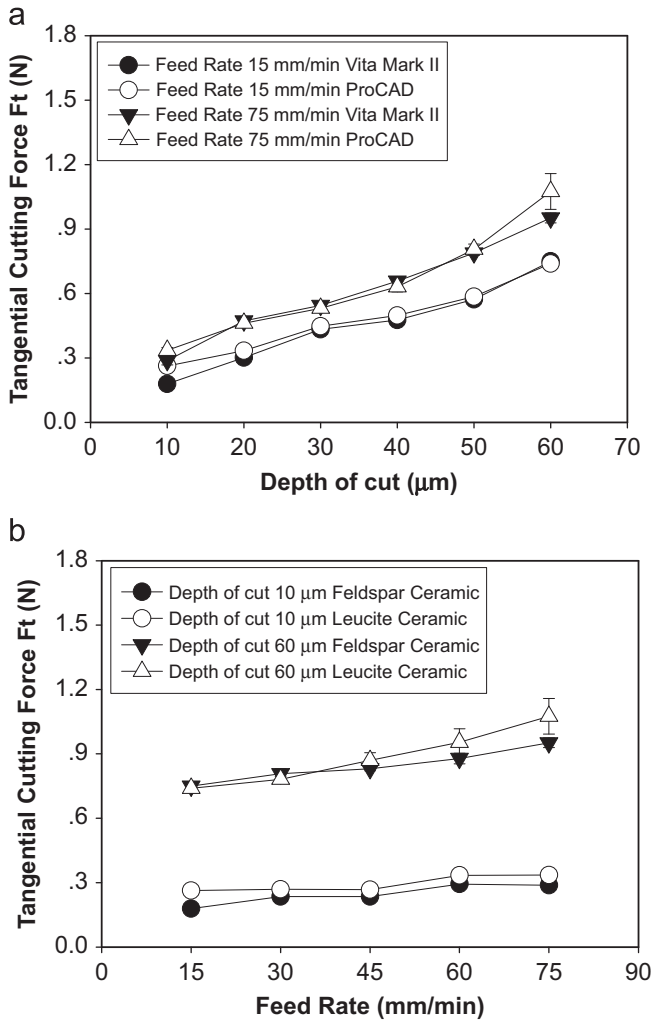

Fig. 3. (a) Tangential cutting force F_t versus depth of cut and (b) tangential cutting force F_t versus feed rate.

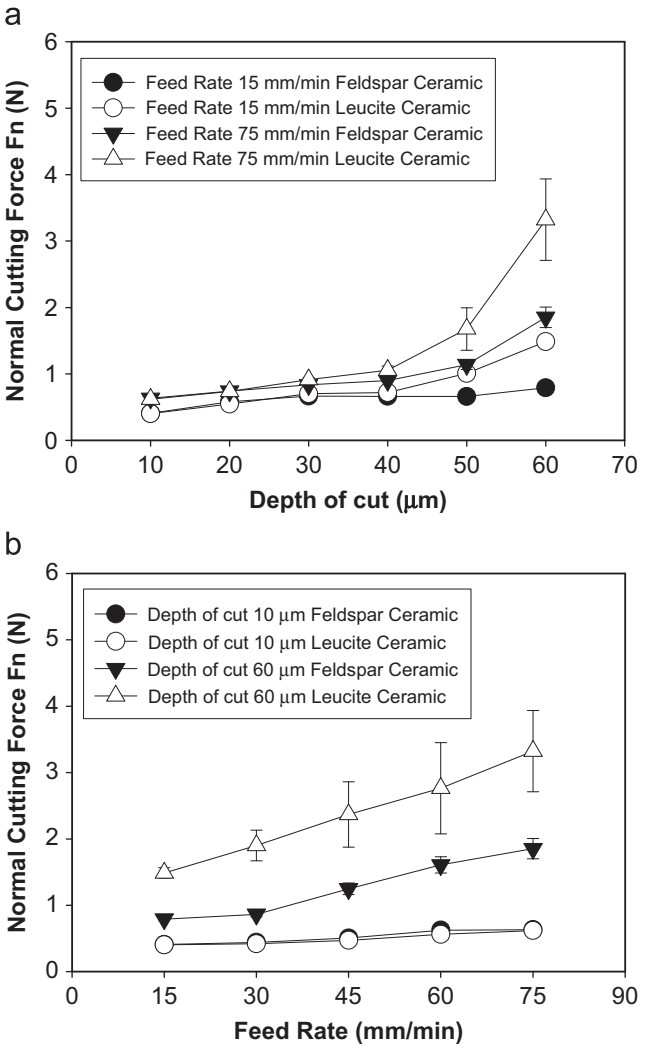

Fig. 4. (a) Normal cutting force F_n versus depth of cut and (b) normal cutting force F_n versus feed rate.

were significantly higher than those for feldspar ceramic, especially at the deeper depth of cuts. Fig. 4(b) shows normal forces versus feed rate for the two materials at the depths of cut of 10 μm and 60 μm. It demonstrates that the forces for both materials increased with the feed rate ($p < 0.01$). At the 10-μm depth of cut, the normal forces for the two materials were very close, reaching approximately 0.4–0.6 N. At the 60-μm depth of cut, the forces for leucite ceramic, scaling 1.49–3.32 N, were much higher than those for feldspar ceramic, ranging 0.79 N–1.85 N.

Force ratios F_n/F_t versus depth of cut for the two materials at the feed rates of 15 m/min and 75 mm/min are shown in Fig. 5(a). It shows that the ratios are in the range of 1–3. The ratios changed irregularly with the depth of cut. Fig. 5(b) shows force ratios F_n/F_t versus feed rate for the two materials at the depths of cut of 10 μm and 60 μm. At 10-μm depth of cut, the force ratios for the two materials did not significantly change with the feed rate ($p > 0.05$). At 60-μm depth of cut, the ratios for the two materials significantly in increased with the feed rate ($p > 0.05$).

3.2. Specific cutting energy

Specific cutting energy versus depth of cut for the two materials at the feed rates of 15 mm/min and 75 mm/min is plotted in Fig. 6(a). For both materials, specific cutting energy decreased with depth of cut ($p < 0.01$). The specific cutting energy values for the two materials were identical at any depth of cut, reaching 20–50 J/mm^3 and 80–180 J/mm^3 at the feed rates of 75 mm/min and 15 mm/min, respectively. Fig. 6(b) shows specific cutting energy versus feed rate for the two materials at the depths of cut of 10 μm and 60 μm. All of them decreased with the feed rate ($p < 0.01$). It is also found that the specific energy at any feed rate for the two materials was very close, reaching 20–80 J/mm^3 and 50–180 J/mm^3 at the depths of cut of 60 μm and 10 μm, respectively.

3.3. Surface roughness and morphology

Arithmetic mean surface roughness R_a values versus depth of cut for the two materials at the feed rates of 15 mm/min

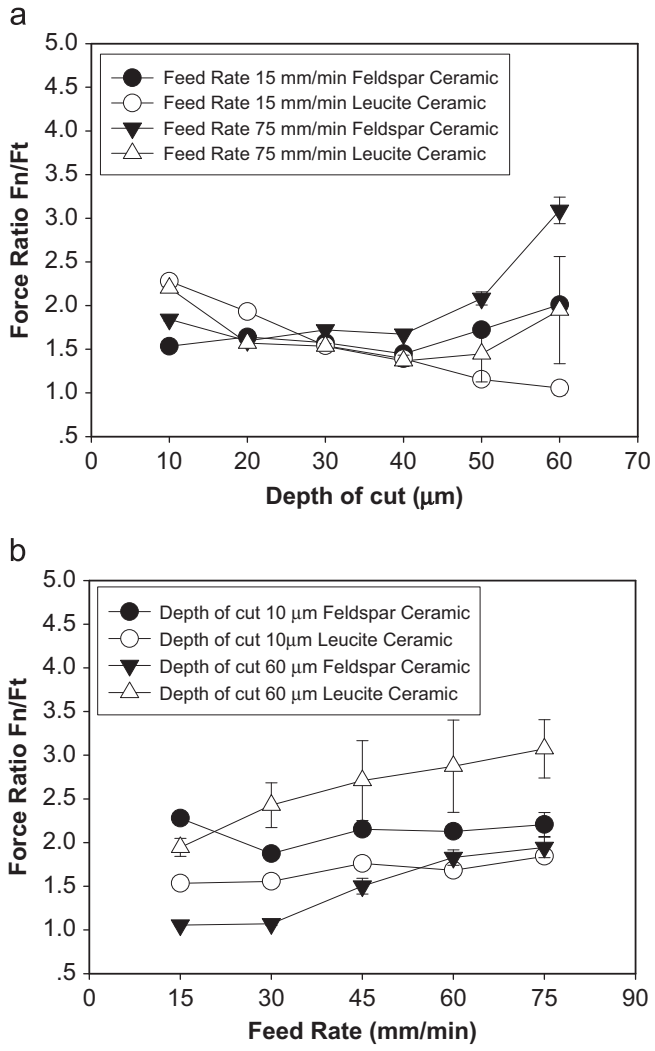

Fig. 5. (a) Force ratio F_n/F_t versus depth of cut and (b) force ratio F_n/F_t versus feed rate.

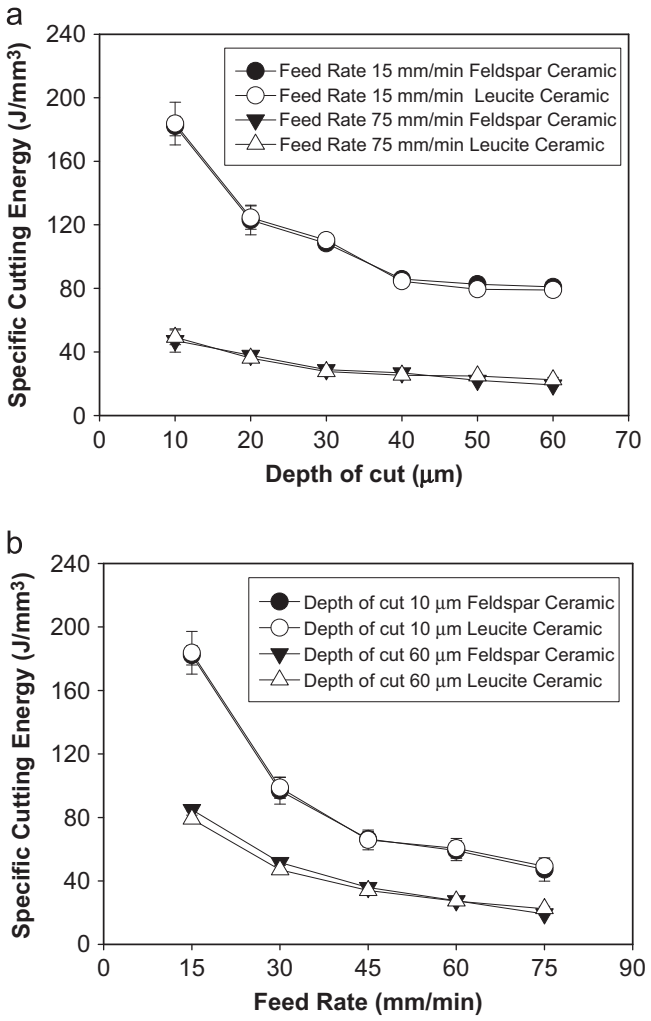

Fig. 6. (a) Specific cutting energy versus depth of cut and (b) specific cutting energy versus feed rate.

and 75 mm/min are shown in Fig. 7(a). The results demonstrate that the R_a values are in the range of 4.5–5.6 μm regardless of the depths of cut. It is also found that that the R_a values for leucite ceramic usually were slightly smaller than those for the feldspar ceramic. The arithmetic mean surface roughness R_a values versus feed rate at the depths of cut of 10 and 60 μm is given in Fig. 7(b). The results show that the R_a values in the range of 4–5.6 μm, apparently independent on the feed rates. It is found that the R_a values for the leucite glass ceramic are generally slightly smaller than those for feldspar glass ceramic in the same cutting conditions ($0.05 > p > 0.01$). ANOVA analyses also demonstrate that the R_a values were not influenced by the depth of cut ($p > 0.05$) and the feed rate ($p > 0.05$).

Maximum roughness R_{max} values versus depth of cut and feed rate are shown in Fig. 8(a) and (b), respectively. The results reveal that the R_{max} values scaled 18–24 μm and were not significantly influenced by either the depth of cut ($p > 0.05$) or the feed rate ($p > 0.05$). The leucite glass ceramic usually exhibited slightly smaller R_{max} values, especially at the higher feed rate of 75 mm/min, compared with feldspar glass ceramic ($0.05 > p > 0.01$).

Fig. 9(a) and (b) shows SEM micrographs of the feldspar and leucite ceramic surfaces machined at the depth of 10 μm and the feed rates of 15 mm/min, respectively. Fig. 9(c) and (d) shows SEM micrographs of the feldspar and leucite ceramic surfaces machined at the depth of 10 μm and the feed rate of 75 mm/min, respectively. Mixtures of brittle fracture and ductile removal are observed on the two material surfaces. At the lower feed rate of 15 mm/min, more ductile removal occurred on both feldspar (Fig. 9(a) and leucite (Fig. 9(b)) ceramic surfaces. At the higher feed rate of 75 mm/min, more brittle fracture and irregular chipping are observed on both materials. At both feed rates, ductile removal was more dominated on the leucite ceramic (Fig. 9(b) and (d)) than the feldspar ceramic (Fig. 9(a) and (c)).

Fig. 10(a) and (b) shows SEM micrographs of the feldspar and leucite ceramic surfaces machined at the depth of 60 μm and the feed rates of 15 mm/min, respectively.

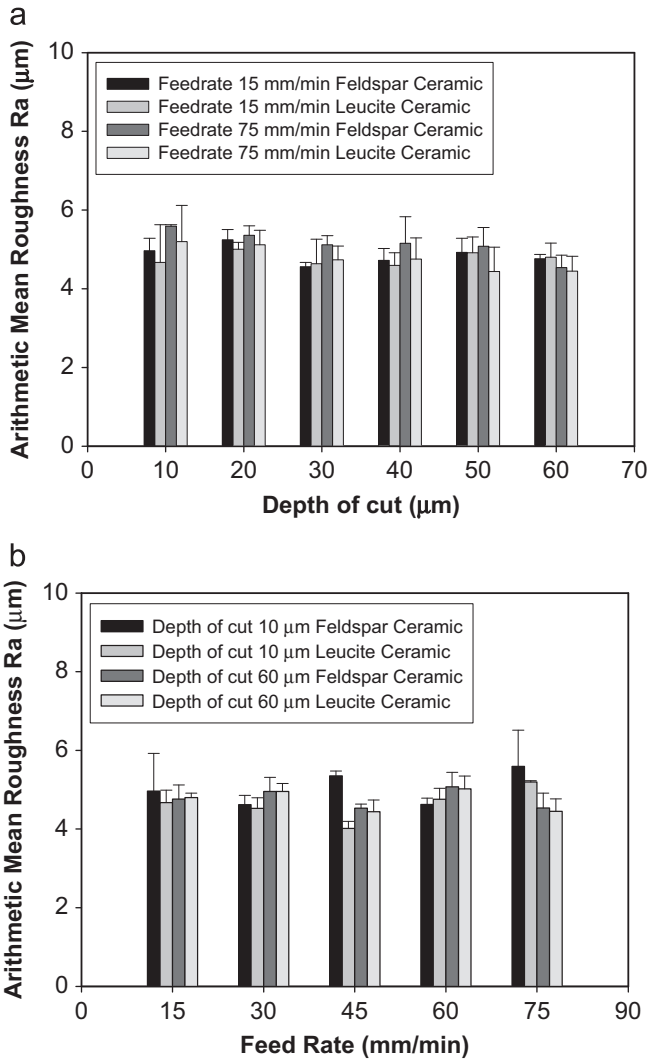

Fig. 7. (a) Arithmetic mean roughness R_a versus depth of cut and (b) arithmetic mean roughness R_a versus feed rate.

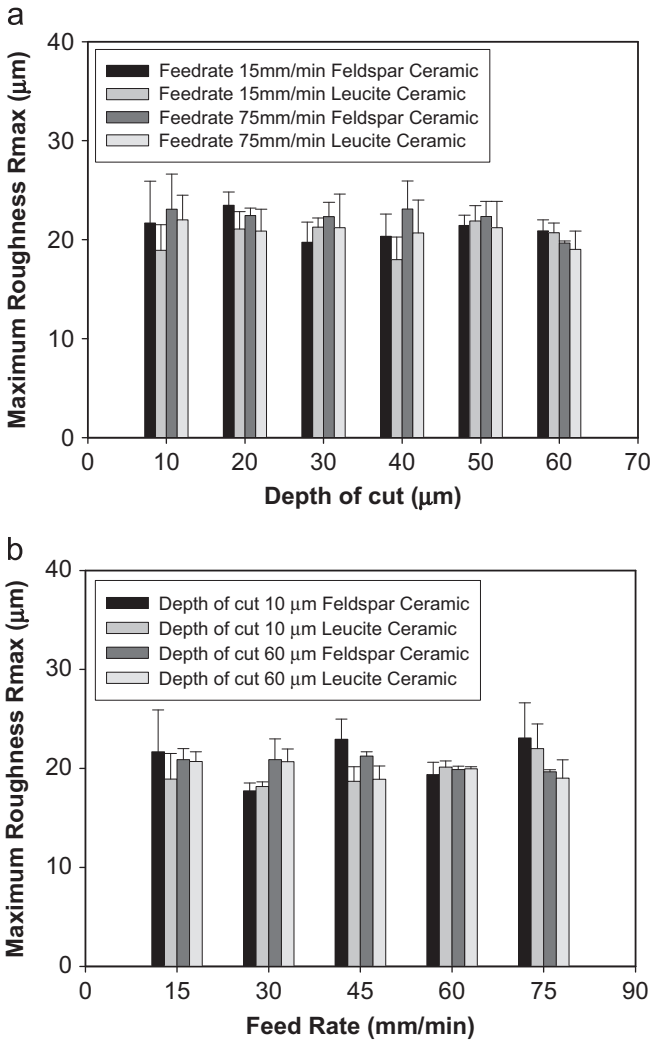

Fig. 8. (a) Maximum roughness R_{max} versus depth of cut and (b) maximum roughness R_{max} versus feed rate.

Fig. 10(c) and (d) shows SEM micrographs of the feldspar and leucite ceramic surfaces machined at the depth of 60 μm and the feed rate of 75 mm/min, respectively. Brittle fracture and localized plastic deformation are found on all surfaces. In comparison to the machined surfaces at the 10-μm depth of cut in Fig. 9, more brittle fracture, chipping and debris are observed on the surfaces machined at the 60-μm depth of cut in Fig. 10. It is also found that more fracture occurred on both ceramic surfaces when increasing the feed rate. Comparing the two ceramics, more brittle fracture is observed on the feldspar ceramic surfaces than that on the leucite ceramic surfaces under the same cutting conditions.

Fig. 11 show details of high-magnification SEM micrographs of the machined feldspar ceramic surfaces. Fig. 11(a) and (b) demonstrates plastic flow at the feed rate of 15 mm/min and mixture of microfracture and fragmentations at the feed rate of 75 mm/min for the depth of 10 μm, respectively. Fig. 11(c) and (d) reveals cleavage and conchoidal fracture at the feed rate of 15 mm/min and large-scale chipping and debris at the feed rate of 75 mm/min for the depth of 60 μm, respectively. Fig. 12 shows details of high-magnification SEM micrographs of the machined leucite ceramic surfaces. Fig. 12(a) and (b) shows plastic flow at the feed rate of 15 mm/min and conchoidal fracture and microfracture at the feed rate of 75 mm/min for the depth of 10 μm, respectively. Fig. 12(c) and (d) demonstrates conchoidal fracture at the feed rate of 15 mm/min and chipping and debris at the feed rate of 75 mm/min for the depth of 60 μm.

Fig. 13 shows SEM topographies of the new and used burs for cutting of feldspar and leucite glass ceramics. Fig. 13(a) and (b) reveals topographies of new burs for feldspar and leucite ceramics, respectively. It is observed that diamond abrasives were clearly deposited on the two new bur surfaces with clean cutting edges. Fig. 13(c) and (d) shows topographies of the used burs for feldspar and leucite ceramics, respectively. Fig. 13(e) and (f) shows high-magnification topographies of used burs for feldspar and leucite ceramics, respectively. It is observed that ceramic debris was loaded on the used burs for both ceramics; especially more debris was loaded on the bur for the leucite

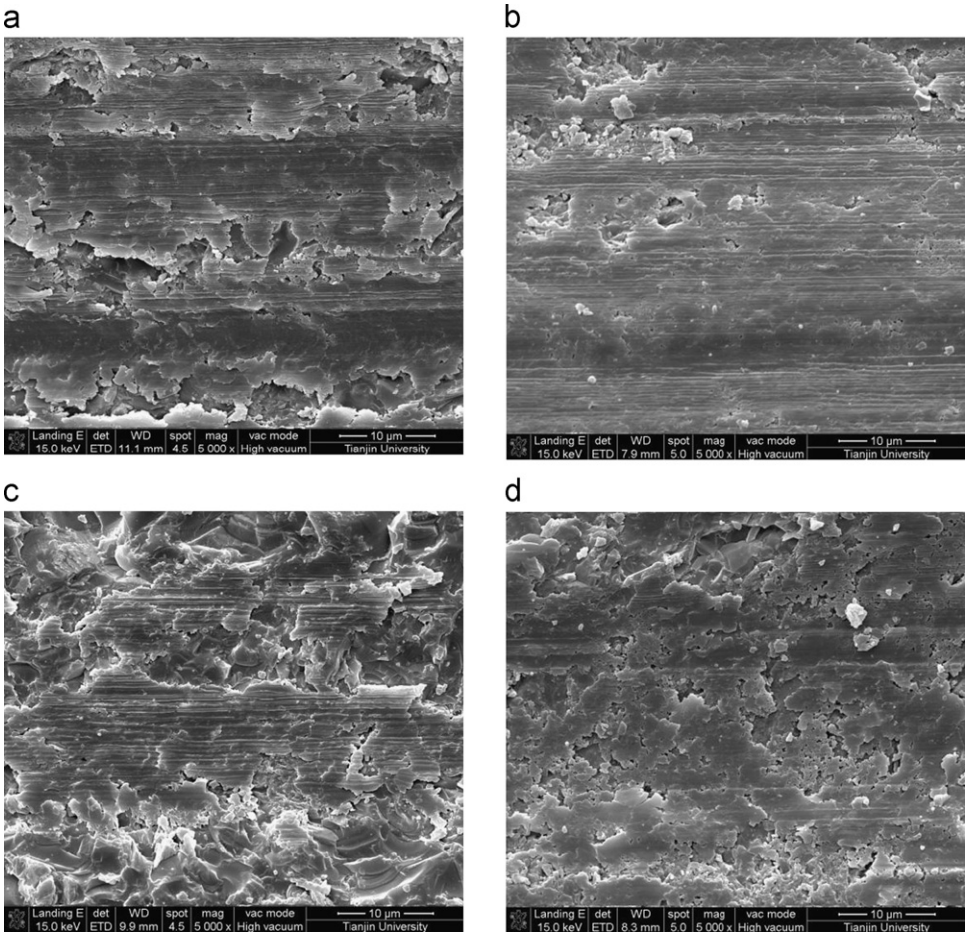

Fig. 9. SEM micrographs of the machined surfaces at the 10-μm depth for the feed rates of (a) 15 mm/min for feldspar glass ceramic, (b) 15 mm/min for leucite glass ceramic, (c) 75 mm/min for feldspar glass ceramic and (d) 75 mm/min for leucite glass ceramic.

ceramic (Fig. 13(f)) than for the feldspar ceramic (Fig. 13(e)). It was also found that some edges of larger diamond grits became clearly more rounded as shown in Fig. 13(e) and (d) due to abrasive wear. No diamond grit pull-out or bond fracture was observed, indicating a good bonding strength at interfaces between diamond grits and the single layered metal bond.

4. Discussion

This research studies the machinability of feldspar and leucite glass ceramics using a high-speed electric motor handpiece and coarse diamond burs under simulated clinical adjusting conditions. Cutting characteristics including forces, force ratios and specific energy, surface roughness and morphology, and bur topographies were assessed. Although feldspar and leucite glass ceramics are ideally restorative materials to meet esthetic demands by scattering light in a manner similar to that of enamel, strength limitations of the two materials are still considered as a distinct disadvantage because of the inherent brittleness of the glass matrix [7]. Due to their intrinsic brittleness, all dental ceramics, especially glass ceramics display low fracture toughness and high failure rates when compared with other dental materials, such as traditional metal-based restorations [34].

Machinability is associated with material properties. Brittleness is normally considered to be an important parameter to estimate machinability of materials [35]. Therefore, the quantification of ceramic brittleness is relevant to assess cutting characteristics in abrasive machining. The index of brittleness, B, associated with the material Vickers hardness, H, and fracture toughness, K_{IC}, is derived as [36]

$$B = H/K_{IC} \tag{2}$$

The indices of brittleness for feldspar and leucite glass ceramics are calculated to be 6.89 $\mu m^{-1/2}$ and 4.31 $\mu m^{-1/2}$, respectively. Higher brittle indices mean that materials are more brittle. Therefore, feldspar ceramic is more brittle than leucite ceramic. A previous study on indices of brittleness for ranking machinable dental materials has showed that there was a perfectly positive correlation between the index of brittleness and the chipping factor. An increase in brittleness resulted in an increase in the potential of marginal chipping [37]. This explains why the machined leucite ceramic surfaces revealed less brittle

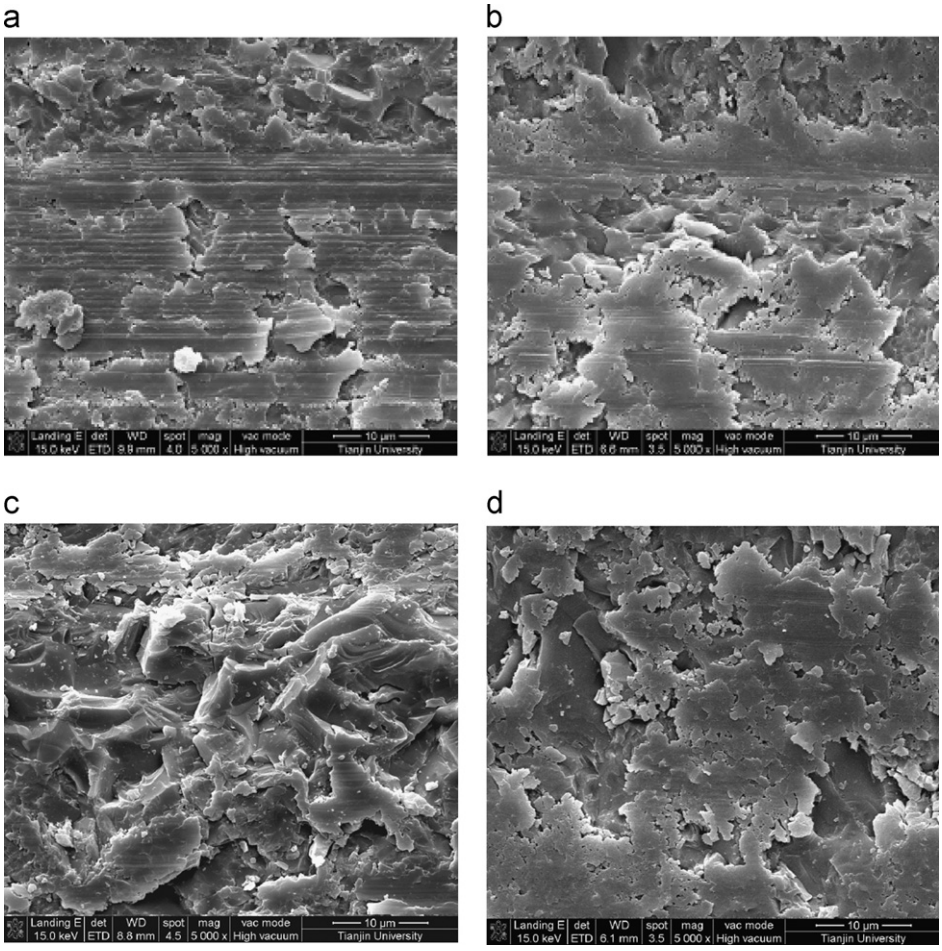

Fig. 10. SEM micrographs of the machined surfaces at the 60-μm depth of cut for the feed rates of (a) 15 mm/min for feldspar glass ceramic, (b) 15 mm/min for leucite glass ceramic, (c) 75 mm/min for feldspar glass ceramic and (d) 75 mm/min for leucite glass ceramic.

fracture than that on feldspar ceramic surfaces due to leucite ceramic's lower index of brittleness.

This study showed that at the slower feed rates or the smaller depths of cut, the cutting mechanics for the two materials revealed similar characteristics in terms of cutting forces (Figs. 3 and 4). However, at the larger feed rates or deeper depths of cut, tangential and normal forces for leucite glass ceramic were higher than those for feldspar glass ceramic. Especially, when the depth of cut was deeper than 50 μm, the normal forces for leucite ceramic were significantly larger compared with the feldspar ceramic (Fig. 4). This can be explained by material removal mechanisms and critical machining forces for brittle–ductile transitions.

In ceramic machining, ceramics are generally removed by brittle fracture. However, when machining forces became very small, ceramics can be removed in a ductile mode without fracture. Based on crack initiation in elastic–plastic indentation fields, the force threshold for the brittle–ductile transition is related to the material properties and can be estimated as [38]

$$P^* = \left(54.47\alpha/\eta^2\theta^4\right)\left(K_{IC}/H\right)^3 K_{IC} \quad (3)$$

where $\alpha = 2/\pi$, $\theta = 0.2$ and $\eta = 1$ for typical intensity and extent of tensile field. The threshold forces P^* for the feldspar and leucite glass ceramic are calculated to be 0.06 N and 0.35 N, respectively.

Abrasive machining can be considered as dynamic indentation processes. Crack initiation and propagation in machining are directly associated with normal forces. SEM micrographs (Figs. 9 and 10) reveal that brittle fracture areas were increased with increased depth of cut and feed rate due to higher normal forces for brittle fracture. At smaller depths of cut or slower feed rates, more plastic deformations were found on the two material surfaces (Fig. 9(a) and (b) and Fig. 10(a) and (b) due to smaller forces for ductile removal. Leucite glass ceramic with a higher threshold force required higher normal forces for crack generation than feldspar ceramic. This explains why normal forces for leucite ceramic were markedly higher than those for feldspar ceramic at the deeper depths of cut.

Furthermore, the cutting process with diamond burs has been customary to consider the scenario in which many individual tips scratch the material surface. Chip generation is controlled by the cutting conditions. At the higher depth of cut or feed rate, more fracture occurred in the cutting

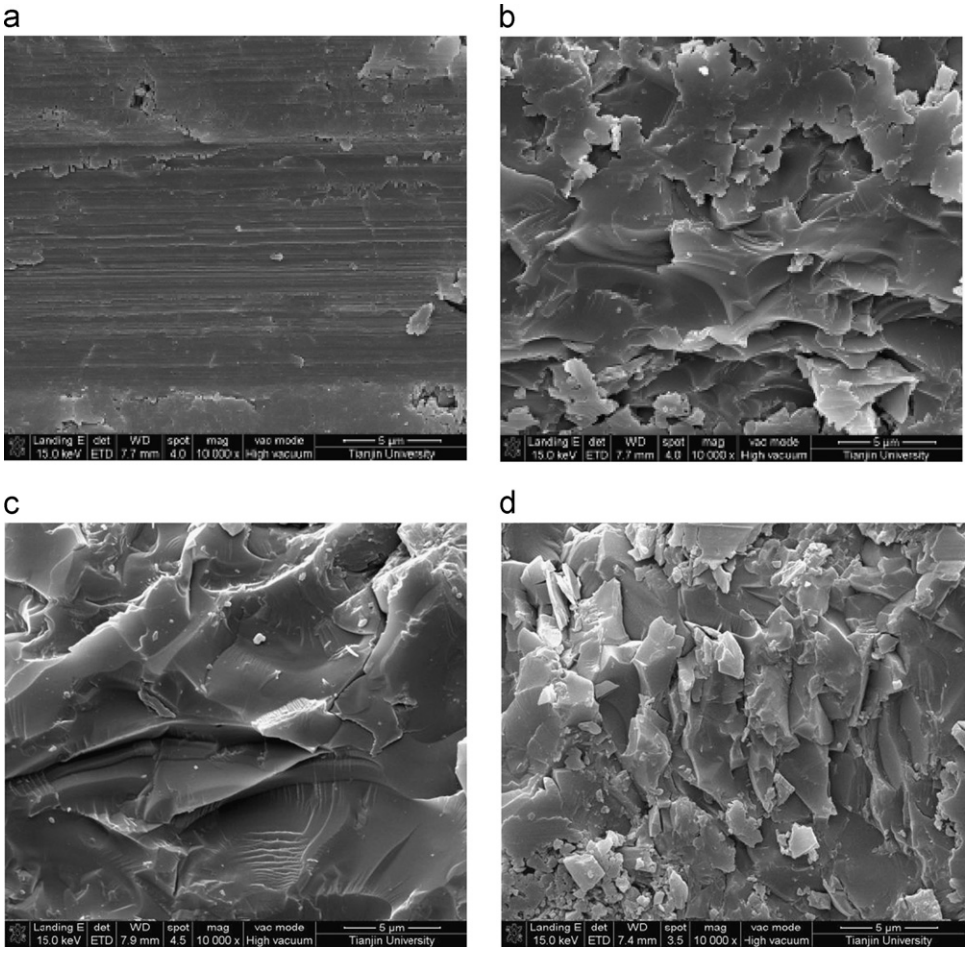

Fig. 11. High-magnification SEM micrographs of the machined surfaces for feldspar ceramic, demonstrating (a) plastic flow at the feed rate of 15 mm/min and (b) mixture of microfracture and fragmentations at the feed rate of 75 mm/min for the depth of 10 μm, (c) cleavage fracture and conchoidal fracture at the feed rate of 15 mm/min and (d) large-scale chipping and debris at the feed rate of 75 mm/min for the depth of 60 μm.

process, resulting in fractured debris at the micro-scale (Fig. 11(c) and (d) for feldspar ceramic and Fig. 12(c) and (d) for leucite glass ceramic). The forces ratios for both materials (Figs. 5 and 6) at higher depth of cut or feed rate became higher, indicating lower frictional coefficients during the cutting process. At the lower depth of cut or feed rate, the plastic removal mode was more dominant in the cutting process, producing highly deformed and smeared debris at the micro or possible nano-scales (Fig. 11(a) for feldspar ceramic and Fig. 12(a) for leucite glass ceramic). These cutting characteristics are similar to the micromechanical and tribological characterization of nano-scale hard amorphous carbon coatings on magnetic recording heads made of alumina–titanium carbide substrate during the diamond scratching process [39]. However, different from the scratching process with a geometry-defined diamond tip, the cutting process with diamond burs with irregular geometries (Fig. 13) is much more complex. At higher removal rates, some abrasives cut the material at the forces below the force threshold for the brittle–ductile transition. At the lower removal rates, more abrasives removed the material under the ductile mode condition due to the lower forces applied.

It is observed that the error bars of cutting forces for the electric handpiece are obviously smaller than those for the air-turbine handpieces under the same dental operational conditions [27]. This indicates that the cutting process using the electric motor handpiece was steadier than those using an air-turbine handpiece. Further, it suggests that the electric handpiece induced more vibration than did the air-turbine handpiece. At the depth of cut of 60 μm and feed rates larger than 60 mm/min, normal forces for leucite ceramic were rapidly increased with a large variation. This means that serious vibration occurred in the cutting process. This phenomenon may be explained with the cutting contact stiffness between the diamond bur and the machined ceramic. The contact stiffness is normally associated with the stiffness of the mechanical system and the normal forces in machining. It can decisively affect the stability of the machining process, i.e., the higher contact stiffness results in more unstable machining processes [40]. In the current dental cutting, a rapid increase in normal forces in cutting leucite ceramic at high removal rate was due to the contact stiffness limit, resulting in the unstable cutting process. This suggests that there

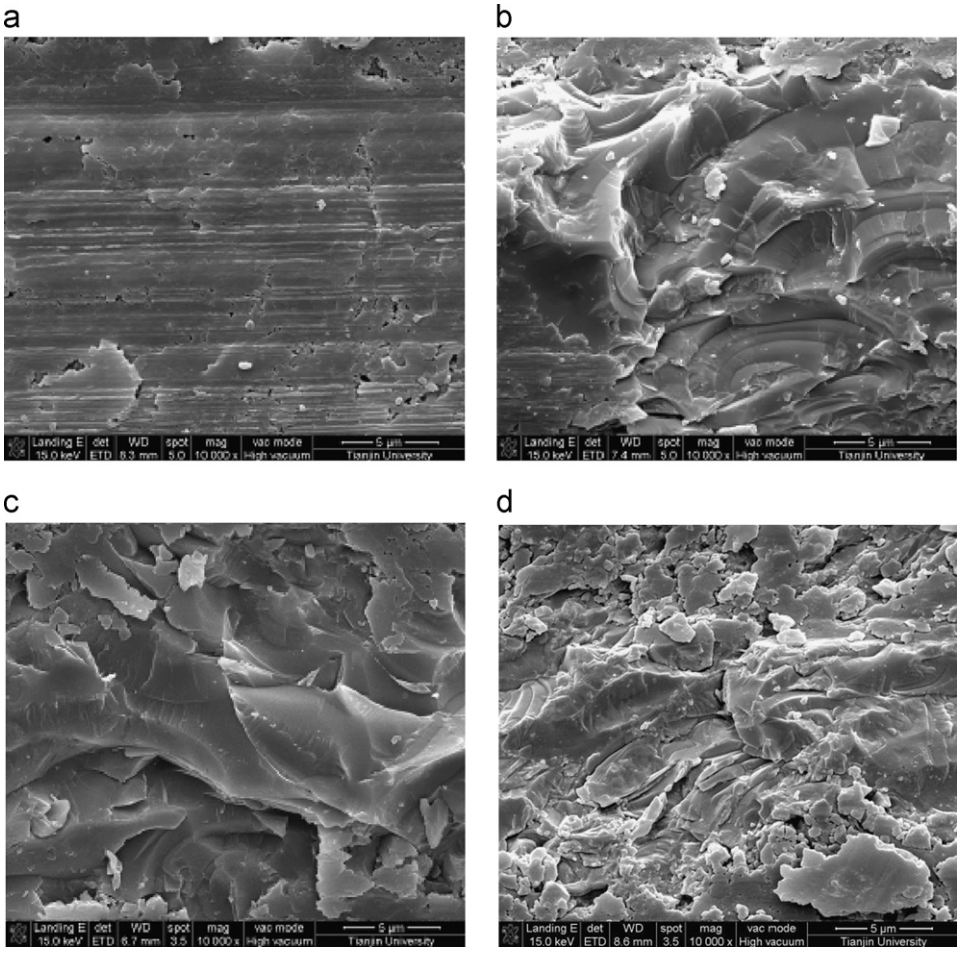

Fig. 12. High-magnification SEM micrographs of the machined surfaces for leucite ceramic, demonstrating (a) plastic flow at the feed rate of 15 mm/min and (b) conchoidal fracture and microfracture at the feed rate of 75 mm/min for the depth of 10 μm; (c) conchoidal fracture at the feed rate of 15 mm/min and (d) chipping and debris at the feed rate of 75 mm/min for the depth of 60 μm.

exists a limitation due to vibration in dental cutting when using an electric handpiece against a ceramic with a high threshold force. In clinical practice, higher removal rates can be constrained because large vibration can be uncomfortable for both dental patients and practitioners.

In abrasive machining, the force ratio F_n/F_t is generally considered to be the inverse ratio of the coefficient of friction, which is an indication of the sharpness of abrasive grits [41]. The typical values of force ratio for ceramic machining were between 3 and 5 [42]. In the current study, the force ratios in dental cutting were about 1–3, smaller than those in conventional machining. This might be attributed to ultra-high rotational speeds of over 200 krpm and extremely small contact zones between the specimen and the small diameter bur in dental cutting. However, force ratios in cutting dental ceramics were larger than the ratios of 1–1.25 in enamel cutting [43]. This is because glass ceramics are much harder than enamel of 3.2 GPa [15]. The harder glass ceramics required higher normal forces for material removal than those of enamel, resulting in larger force ratios in cutting.

Specific energy is mainly consumed by ductile deformation, which is a direct indication of material removal mechanism [44,45]. This study found that ductile deformation areas were rapidly increased with the decreased depth of cut or feed rate for both materials (Figs. 9 and 10). Consequently, the specific energy showed significant downtrend with the increase in depth of cut or the feed rate. Specific energy is generally considered to be related to a grit depth of cut taken by an individual cutting point in abrasive machining, i.e., the maximum undeformed chip thickness h_{max}. The maximum undeformed chip thickness h_{max} can be calculated as [33]

$$h_{max} = (3/Ctan\theta)^{1/2}(v_w/v_s)^{1/2}(a/d_s)^{1/4} \quad (4)$$

where C is the number of active cutting points per unit area, θ is the semi-included angle for the undeformed chip, v_w is the bur feed rate, v_s is the bur peripheral speed, a is the depth of cut, and d_s is the bur diameter. For the bur with a 106–125 μm grit size, C is taken as 20 and θ as 60° [33,46].

Specific cutting energy versus maximum undeformed chip thickness is shown in Fig. 14. It shows that the specific energy had an inverse dependence on the

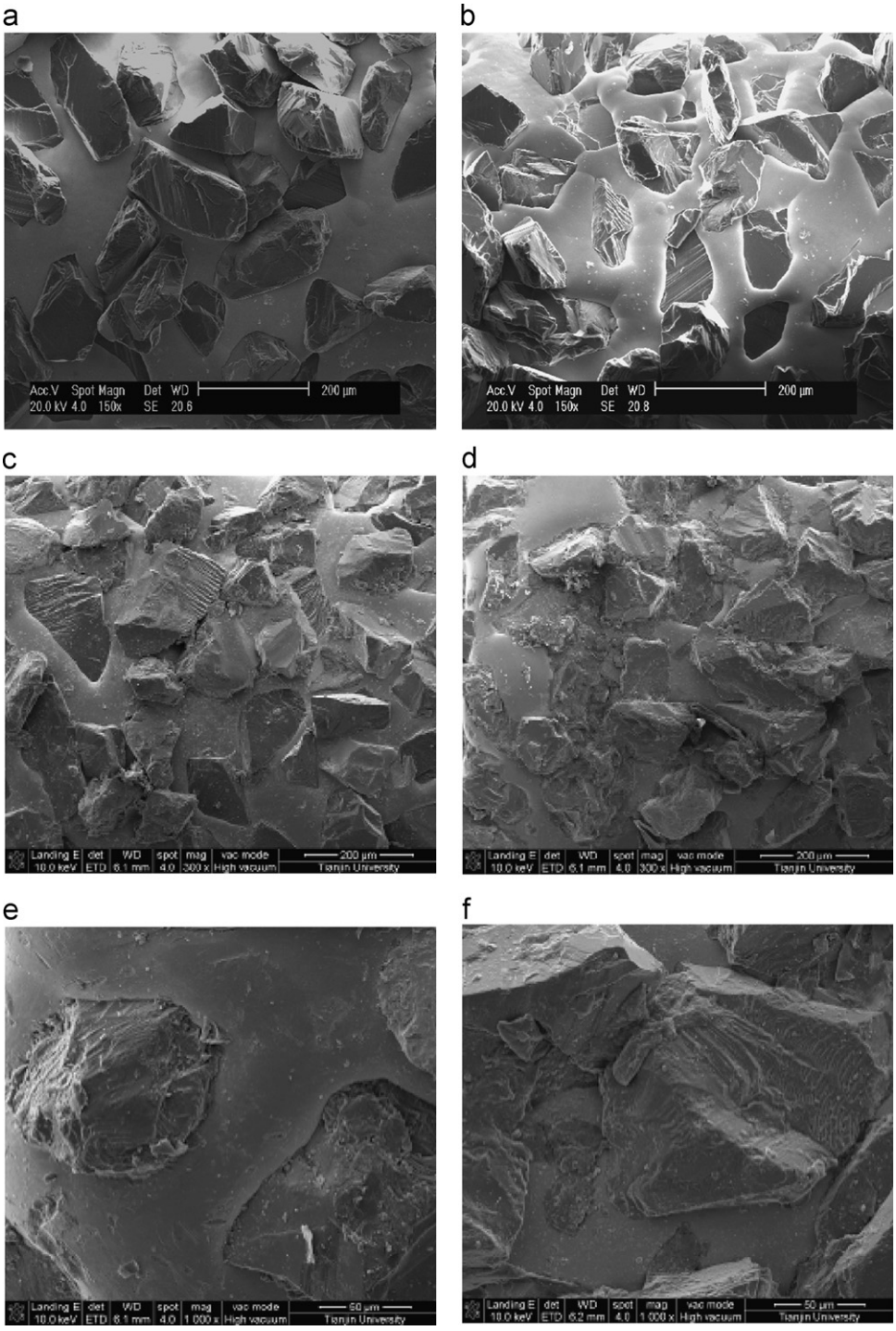

Fig. 13. SEM micrographs of the new burs for cutting (a) feldspar and (b) leucite glass ceramics, and the used burs for cutting (c) feldspar and (d) leucite glass ceramics at a low magnification, and details of the used bur for cutting (e) feldspar and (f) leucite glass ceramics.

maximum undeformed chip thickness. This is in agreement with the common findings in conventional ceramic machining where increasing undeformed chip thickness resulted in a reduction in specific machining energy [47,48].

It is interesting to find that surface roughness in dental cutting was not necessarily affected by process parameters such as depth of cut or feed rate and materials. However, SEM surface morphologies exhibited a certain dependence on cutting conditions and materials (Figs. 9 and 10). As both ductile deformation and brittle fracture were involved in cutting the two materials, surface morphologies of the two machined materials featured a mixture of ductile and brittle removal. Decreasing cutting forces due to smaller depths of cut or feed rate resulted in the visible brittle–ductile transitions for both materials (Fig. 9(a) and (b)). In contrast, with increasing cutting forces at larger depths of

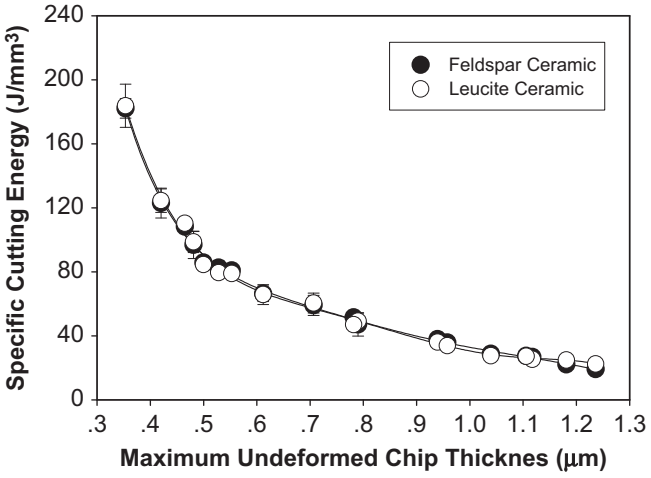

Fig. 14. Specific cutting energy versus maximum undeformed chip thickness.

cut and feed rates, more machined surfaces were generated by brittle fracture (Fig. 10(c) and (d)).

It is also of interest in fracture features to approach material removal mechanisms. In both materials, reinforced crystalline phases formed randomly in glass matrices. However, interfaces between feldspar or leucite crystals and glass phases were not visible. Cleavage and conchoidal fractures together with irregular chipping were the dominant fracture features (Figs. 11 and 12). The cleavage fracture may be due to tensile stresses acting normal to low-bonding crystalline phases. The conchoidal fracture is similar to the fracture feature in amorphous glasses or solids with cracks proceeding normal to the applied tension [49]. This indicates that the fracture removal process was mainly originated from transgranular fracture and irregular lateral or median crack chipping [48]. This finding is consistent with the previous studies on cutting of dental ceramics using air-turbine handpieces and coarse diamond burs, where extensive chipping damage due to the extension of lateral/median cracks was observed [33,49]. It should also be noted that these brittle fracture or other machining-induced flaws could greatly affect the mechanical strength of finished ceramic prostheses [14,50]. Therefore, to obtain high quality ceramic restorations for clinical demand, these surface damages should be removed by fine polishing using finer grit dental burs.

5. Conclusions

This research evaluated of machiniability of dental ceramics in clinical adjusting process by characterizing *in vitro* cutting of feldspar and leucite glass ceramics using an electric handpiece and coarse diamond burs. The results show that tangential and normal forces and specific cutting energy for the two materials were significantly affected by the cutting parameters of the bur ($p < 0.01$). However, surface roughness for both the materials was not sensitive to the applied cutting conditions ($p > 0.05$). Similarities in tangential and normal forces and specific cutting energy between the two materials were found only at low feed rates or small depths of cut ($p > 0.05$). Significantly higher normal forces were measured in cutting leucite glass ceramic at larger feed rates or deeper depths of cut ($p < 0.05$). Both material surface morphologies were featured with plastic deformation, brittle fracture and chipping. However, the machined leucite glass ceramic revealed less brittle fracture due to its lower index of brittleness and higher force threshold for brittle–ductile transition. Leucite-reinforced ceramic exhibited improved cutting surfaces due to its higher density of discontinuing ductile regions in comparison with the feldspar glass ceramic. This study contributed to establishing fundamental quantitative evaluation and understanding of machinability of dental ceramics in materials selection, processing and quality control in clinical dentistry.

Acknowledgments

This work was supported by the National Natural Science Foundation of China (Grant no. 50905124) and the Specialized Research Fund for the Doctoral Program of Higher Education of China (Grant no. 20090032120011).

References

[1] J.R. Kelly, P. Benetti, Ceramic materials in dentistry: historical evolution and current practice, Australian Dental Journal 56 (1) (2011) 84–96.
[2] A.R. Studart, F. Filser, P. Kocher, L.J. Gauckler, *In vitro* lifetime of dental ceramics under cyclic loading in water, Biomaterials 28 (2007) 2695–2705.
[3] J.A. Griggs, Recent advances in materials for all-ceramic restorations, Dental Clinics of North America 51 (3) (2007) 713–727.
[4] K.J. Anusavice, Standardizing failure, success, and survival decisions in clinical studies of ceramic and metal–ceramic fixed dental prostheses, Dental Materials 28 (1) (2012) 102–111.
[5] W. Höland, V.M. Rheinberger, E. Apel, C. van't Hoen, M. Höland, A. Dommann, M. Obrecht, C. Mauth, U. Graf-Hausner, Clinical application of glass-ceramics in dentistry, Journal of Materials Science: Materials in Medicine 17 (2006) 1037–1042.
[6] H. Yilmaz, C. Aydin, B.E. Gul, Flexual strength and fracture toughness of dental core ceramics, Journal of Prosthetic Dentistry 98 (2007) 120–128.
[7] A. Shenoy, N. Shenoy, Dental ceramics: an update, Journal of Conservative Dentistry 13 (4) (2010) 195–203.
[8] E.D. Rekow, N.R.F.A. Silva, P.G. Coelho, Y. Zhang, P. Guess, V.P. Thompson, Performance of dental ceramics: challenges for improvements, Journal of Dental Research 90 (8) (2011) 937–952.
[9] D. Layton, T. Walton, An up to 16-year prospective study of 304 porcelain veneers, International Journal of Prosthodontics 20 (4) (2007) 389–396.
[10] M. Fradeani, M. Redemagni, M. Corrado, Porcelain laminate veneers: 6 to 12 year clinical evaluation—a retrospective study, International Journal of Periodontics and Restorative Dentistry 25 (1) (2005) 9–17.
[11] M. Fradeani, Six-year follow-up with empress veneers, International Journal of Periodontics and Restorative Dentistry 18 (3) (1998) 216–225.
[12] B.R. Lawn, A. Pajares, Y. Zhang, Y. Deng, M.A. Polack, I.K. Lloyd, E.D. Rekow, V.P. Thompson, Materials design in the performance of all-ceramic crowns, Biomaterials 25 (2004) 2885–2892.

[13] M. Kikuchi, The use of cutting temperature to evaluate the machinability of titanium alloys, Acta Biomaterialia 5 (2009) 770–775.
[14] M. Guazzato, M. Albakry, L. Quach, M.V. Swain, Influence of grinding, sandblasting, polishing and heat treatment on the flexural strength of a glass-infiltrated alumina-reinforced dental ceramic, Biomaterials 25 (2004) 2153–2160.
[15] L. Yin, X.F. Song, Y.L. Song, T. Huang, J. Li, An overview of *in vitro* abrasive finishing and CAD/CAM of bioceramics in restorative dentistry, International Journal of Machine Tools and Manufacture 46 (9) (2006) 1013–1026.
[16] S.C. Siegel, J.A. von Fraunhofer, Dental cutting: the historical development of diamond burs, Journal of the American Dental Association 129 (6) (1998) 740–745.
[17] C.W. Chang, J.N. Waddell, K.M. Lyons, M.V. Swain, Cracking of porcelain surfaces arising from abrasive grinding with a dental air turbine, Journal of Prosthodontics 20 (8) (2011) 613–620.
[18] X.F. Song, L. Yin, Y.G. Han, H. Wang, *In vitro* rapid adjustment of porcelain prostheses using a high-speed dental handpiece, Acta Biomaterialia 4 (2) (2008) 414–424.
[19] Y. Zhang, B.R. Lawn, E.D. Rekow, V.P. Thompson, Effect of sandblasting on the long-term performance of dental ceramics, Journal of Biomedical Materials Research 71B (2004) 381–386.
[20] G.J. Christensen, Are electric handpieces an improvement?, Journal of the American Dental Association 133 (2002) 1433–1434
[21] G.J. Christensen, The high-speed handpiece dilemma, Journal of the American Dental Association 130 (1999) 1494–1496.
[22] T.M. Roberson, H.O. Heymann, E.J. Swift Jr., Instruments and equipment for tooth preparation, in: T.M. Roberson (Ed.), Sturdevant's Art and Science of Operative Dentistry, Mosby, St. Louis, 2002, pp. 322–329.
[23] S. Eikenberg, D. Roman, R. Debuque, et al., A comparison and evaluation of electric motor dental handpieces and air turbine dental handpieces, Great Lakes, Ill, United States Army Dental Research Attachment, Protocol, 451, 2000, pp. 1–75.
[24] B.J. Kenyon, I. Van Zyl, K.J. Louie, Comparison of cavity preparation quality using an electric motor handpiece and an air turbine dental handpiece, Journal of the American Dental Association 136 (2005) 1101–1105.
[25] C. Choi, C.F. Driscoll, E. Romberg, Comparison of cutting efficiencies between electric and air-turbine dental handpieces, The Journal of Prosthetic Dentistry 103 (2010) 101–107.
[26] C. Ercoli, M. Rotella, P.D. Funkenbusch, S. Russell, C. Feng, *In vitro* comparison of the cutting efficiency and temperature production of ten different rotary cutting instruments. Part II: electric handpiece and comparison with turbine, The Journal of Prosthetic Dentistry 101 (2009) 319–331.
[27] L. Yin, X.F. Song, S.F. Qu, Y.G. Han, H. Wang, Surface integrity and removal mechanism in simulated dental finishing of a feldspathic porcelain, Journal of Biomedical Materials Research Part B: Applied Biomaterials 79B (2006) 365–378.
[28] I.M. Peterson, A. Pajares, B.R. Lawn, V.P. Thompson, E.D. Rekow, Mechanical characterization of dental ceramics by Hertzian contacts, Journal of Dental Research 77 (1998) 589–602.
[29] Y. Deng, B.R. Lawn, I.K. Lloyd, Characterization of damage modes in dental ceramic bilayer structures, Journal of Biomedical Materials Research Part B: Applied Biomaterials 63 (2002) 137–145.
[30] R. Giordano, Materials for chariside CAD/CAM-produced restorations, Journal of the American Dental Association 137 (2006) 14S–21S.
[31] A. Bindl, H. Lüthy, W.H. Mörmann, Strength and fracture pattern of monolithic CAD/CAM-generated posterior crowns, Dental Materials 22 (2006) 29–36.
[32] L. Yin, X.F. Song, S.F. Qu, T. Huang, J.P. Mei, Z.Y. Yang, J. Li, Performance evaluation of a dental handpiece in simulation of clinical finishing using a novel 2DOF *in vitro* apparatus, Proceedings of the Institution of Mechanical Engineers—Part H: Journal of Engineering in Medicine 220 (2006) 929–938.
[33] S. Malkin, Grinding Technology: Theory and Applications of Machining with Abrasives, Wiley, New York, 1989.
[34] A.S. Rizkalla, D.W. Jones, Indentation fracture toughness and dynamic elastic moduli for commercial feldspathic dental porcelain materials, Dental Materials 20 (2004) 198–206.
[35] A.R. Boccaccini, Machinability and brittleness of glass-ceramics, Journal of Materials Processing Technology 65 (1997) 302–304.
[36] B.R. Lawn, D.B. Marshall, Hardness, toughness and brittleness-indentation analysis, Journal of the American Ceramic Society 62 (1979) 347–350.
[37] E.A. Tsitrou, S.E. Northeast, R. van Noort, Brittleness index of machinable dental materials and its relation to the marginal chipping factor, Journal of Dentistry 35 (2007) 897–902.
[38] B.R. Lawn, A.G. Evans, A model for crack initiation in elastic/plastic indentation fields, Journal of Materials Science 12 (1977) 2195–2199.
[39] X.D. Li, B. Bhushan, Micromechanical and tribological characterization of hard amorphous carbon coatings as thin as 5 nm for magnetic recording heads, Wear 220 (1998) 51–58.
[40] I. Inasaki, H.R. Meyer, F. Klocke, J. Shibata, G. Spur, H.K. Tonshoff, H.G. Wobker, Grinding, in: I.D. Marinescu, H.K. Tonshoff, I. Inasaki (Eds.), Handbook of Ceramic Grinding and Polishing, Noyes Publications, Park Ridge, New Jersey, 2000, pp. 194–200.
[41] I.D. Marinescu, B. Dimitrov, I. Inasaki, Tribology of Abrasive Machining Processes, Villiam Andrew, New York, 2004.
[42] L. Yin, H. Huang, K. Ramesh, T. Huang, High speed versus conventional grinding in high removal rate machining of alumina and alumina–titania, International Journal of Machine Tools and Manufacture 45 (2005) 897–907.
[43] I.A.N. Westland, The energy requirement of the dental cutting process, Journal of Oral Rehabilitation 7 (1980) 51–63.
[44] T.W. Hwang, S. Malkin, Upper bound analysis for specific energy in grinding of ceramics, Wear 231 (1999) 161–171.
[45] T.W. Hwang, S. Malkin, Grinding mechanisms and energy balance for ceramics, Journal of Manufacturing Science and Engineering 121 (1999) 623–631.
[46] T.W. Hwang, C.J. Evans, S. Malkin, Size effect for specific energy in grinding of silicon nitride, Wear 225–229 (1999) 862–867.
[47] S. Malkin, T.W. Hwang, Grinding mechanisms for ceramics, CIRP Annals—Manufacturing Technology 45 (1996) 569–580.
[48] C. Barry Carter, M. Grant Norton (Eds.), Ceramic Materials: Science and Engineering, Springer, Berlin, 2007.
[49] X.F. Song, L. Yin, Surface morphology and fracture in handpiece adjusting of a leucite-reinforced glass ceramic with coarse diamond burs, Materials Science and Engineering: A 534 (1) (2012) 193–202.
[50] T. Asai, R. Kazama, M. Fukushima, T. Okiji, Effect of overglazed and polished surface finishes on the compressive fracture strength of machinable ceramic materials, Dental Materials Journal 29 (2010) 661–667.